Polarization-independent self-collimation based on pill-void photonic crystals with square symmetry

Yi Xu, Xiao-Jun Chen, Sheng Lan, Qiao-Feng Dai, Qi Guo and Li-Jun Wu*

Laboratory of Photonic Information Technology, School for Information and Optoelectronic Science and Engineering, South China Normal University, Guangzhou 510006, P.R. China

*Corresponding author: ljwu@scnu.edu.cn

Abstract: We investigate discrepancy and similarity in dispersion relations between transverse-electric (TE) and transverse-magnetic (TM) polarizations in rectangular, square and triangular two-dimensional photonic crystals. It is found that the square lattice is the most appropriate candidate to realize polarization-independent, i.e. absolute self-collimation (ASC) in the first photonic band since it possesses not only a relatively broad angular range for self-collimation but also a small difference in dispersion relations between TE and TM modes. By tailoring the shape of air voids in the square-lattice-based structure, the electric-field vector can be rotated to reduce the discrepancy between TE and TM modes whereby the frequency bandwidth of ASC can be enlarged to ~4.8%. The ASC phenomenon is demonstrated by numerical experiments based on a finite-difference time-domain (FDTD) technique with negligible propagation losses.

©2009 Optical Society of America

References and links

1. E. Yablonovitch, "Inhibited spontaneous emission in solidstate physics and electronics," Phys. Rev. Lett. **58**, 2059-2062 (1987).
2. S. John, "Strong Localization of Photons in Certain Disordered Dielectric Superlattices," Phys. Rev. Lett., **58**, 2486-2489 (1987).
3. H. G. Park, S. H. Kim, S. H. Kwon, Y. G. Ju, J. K. Yang, J. H. Baek, S. B. Kim, and Y. H. Lee, "Electrically driven single-cell photonic crystal laser," Science **305**, 1444–1447 (2004).
4. L. H. Frandsen, A. Harpoth, P. I. Borel, M. Kristensen, J. S. Jensen, and O. Sigmund, "Broadband photonic crystal waveguide 60 degrees bend obtained utilizing topology optimization," Opt. Express **12**, 5916–5921 (2004), http://www.opticsexpress.org/abstract.cfm?URI=OPEX-12-24-5916.
5. Y. Yasha, B. Peter, W. Kazumi, D. Xiaoman, J. D. Joannopoulos, and L. C. Kimerling, "Tunable multichannel optical filter based on silicon photonic band gap materials actuation," Appl. Phys. Lett., **81**, 4112-4114 (2002).
6. H. Kosada, T. Kawashima, A. Tomita, M. Notomi, T. Tamamura, T. Sato, and S. Kawakami, "Superprism phenomena in photonic crystals," Phys. Rev. B **58**, 10096-10099 (1998).
7. L. Wu, M. Mazilu, T. Karle, and T. F. Krauss, "Superprism Phenomena in Planar Photonic Crystals," IEEE J. Quantum Electron. **38**, 915-918 (2002).
8. L. Wu, M. Mazilu, J. F. Gallet, and T. F. Krauss, "Dual lattice photonic-crystal beam splitters," Appl. Phys. Lett. **86**, 211106-211109 (2005).
9. H. Kosaka, T .Kawashima, A. Tomita, M. Notomi, T. Tamamura, T. Sato, and S. Kawakamib, "Self-collimating phenomena in photonic crystals," Appl. Phys. Lett. **74**, 1212-1214 (1999).
10. C. Luo, S. G. Johnson, J. D. Joannopoulos, and J. B. Pendry, "All-angle negative refraction without negative effective index," Phys. Rev. B **65**, 201104(R) (2002).
11. C. Luo, S. G. Johnson, J. D. Joannopoulos, and J. B. Pendry, "All-angle negative refraction in a three-dimensionally periodic," Appl. Phys. Lett. **81**, 2352-2354 (2002).
12. L. Wu, M. Mazilu, and T. F. Krauss, "Beam Steering in Planar-Photonic Crystals: From Superprism to Supercollimator," J. Lightwave Technol. **21**, 561-566 (2003).

13. J. Witzens, M. Loncar, and A. Schere, "Self-collimation in planar photonic crystals," IEEE J. Sel. Top. Quantum Electron. **8**, 1246-1257 (2002).
14. D. N. Chigrin, S. Enoch, C. M. S. Torres, and G. Tayeb, "Self-guiding in two-dimensional photonic crystals," Opt. Express **11**, 1203-1211 (2003).
15. D. W. Prather, S. Shi, D. M. Pustai, C. Chen, S. Venkataraman, A. Sharkawy, G. J. Schneider, and J. Murakowski, "Dispersion-based optical routing in photonic crystals," Opt. Lett. **29**, 50-52 (2004).
16. P. T. Rakich, M. S. Dahlem, S. Tandon, M. Ibanescu, M. SoljaČiĆ, G. S. Petrich, J. D. Joannopoulos, L. A. Kolodziejski, and E. P. Ippen, "Achieving centimeter-scale supercollimation in a large-area two-dimensional photonic crystal" Nature Mater. **5**, 93-96 (2006).
17. D. W. Prather, S. Shi, J. Murakowski, G. J. Schneider, A. Sharkawy, C. Chen, B. Miao, and R. Martin, "Self-collimation in photonic crystal structures: a new paradigm for applications and device development," J. Phys. D **40**, 2635-2651 (2007).
18. V. Zabelin, L. A. Dunbar, N. Le. Thomas, R. Houdré, M. V. Kotlyar, L. O'Faolain, and T. F. Krauss, "Self-collimating photonic crystal polarization beam splitter," Opt. Lett., **32**, 530-532 (2007).
19. Yi Xu, Xiao-Jun Chen, Sheng Lan, Qi Guo, Wei Hu, and Li-Jun Wu, "The all-angle self-collimating phenomenon in photonic crystals with rectangular symmetry," J. Opt. A **10** 085201 (2008).
20. S. G. Johnson and J. D. Joannopoulos, "Block-iterative frequency-domain methods for Maxwell's equations in a planewave basis," Opt. Express **8**, 173 (2001), http://www.opticsexpress.org/abstract.cfm?URI=OPEX-8-3-173.
21. J. D. Joannopoulos, R. D. Meade, and J. N. Winn, *Photonic Crystals: Molding the Flow of Light* (Princeton University Press, Princeton, 1995).
22. N. Susa, "Large absolute and polarization-independent photonic band gaps for various lattice structures and rod shapes," J. Appl. Phys. **91**, 3501-3510 (2002).
23. T. Baba and D. Ohsaki, "Interfaces of photonic crystals for high efficiency light transmission," Jpn. J. Appl.Phys. **40**, 5920-5924 (2001).

1. Introduction

Photonic crystals (PhCs) [1, 2] are a novel class of composite materials which provide the opportunity to control electromagnetic (EM) flows. They are periodic dielectric distributions on a length scale comparable to the wavelength of the incident light. Interference of the light waves scattered from the dielectric lattice leads to photonic bandgaps (PBGs). Many of the studies on PhCs have focused on the means of tailoring the emission and propagation of light using PBG property whereby the photon density of states is zero. For example, low threshold lasing [3], high efficiency broadband wave guiding [4] and filtering [5] etc. have been proposed and investigated based on this significant phenomenon. On the other hand, PhCs have another attractive property—abnormal refraction. This phenomenon has attracted a lot of attention because of its potential applications in photonic integrated circuits [6-8]. For example, Kosaka et al. have introduced the so-called "superprism phenomenon" [6] and "self-collimating phenomenon" in PhCs [9]. Luo et al have suggested that all angle negative refraction exists in both two-dimensional (2D) and three-dimensional (3D) PhCs [10, 11]. Such kinds of abnormal refraction provide ways to control EM waves artificially by engineering the dielectric distributions and essentially the equi-frequency contours (EFCs) of PhCs.

Diffraction of EM waves occurs in uniform linear dielectric media and leads to significant spreading of the optical beams as they propagate. Self-collimating phenomenon in PhCs means that the energy propagation directions for all the excited modes are identical and the diffraction can be almost eliminated. This behavior was initially demonstrated by Kosaka et al [9] and Wu et al [12] in 3D and 2D PhCs, respectively. However, most of the research on self-collimation has focused only on a certain polarized wave, the transverse-electric (TE) or transverse-magnetic (TM) polarization [9, 12-17]. From the viewpoint of facilitating synchronous functions for both polarizations, it will be very useful if polarization-independent, i.e. absolute self-collimation (ASC) with low propagation losses can be realized in PhCs. Recently, Zabelin et al demonstrated a PhC polarization beam splitter in the 2D square lattice in which both polarizations can be collimated [18]. However, the transmission of their device does not meet the demand for practical applications because it operates above the light cone in the second photonic band and suffers from intrinsic out-of-plane scattering losses.

In this paper, we will demonstrate the ASC phenomenon in a 2D square-lattice-based structure operating in the first band which is below the light cone by theoretical analysis and numerical simulation. By changing the shape of the air-void from circle to pill, the frequency bandwidth of ASC can be enlarged from ~1.6% to ~4.8%, which is sufficient for applications in optical integrated circuits. The rest of this paper is organized as follows. In Sec. 2, we will discuss the discrepancy in dispersion relations between TE (electric-field parallel to the plane) and TM (magnetic-field parallel to the plane) polarizations in rectangular, square and triangular lattices of circular air voids in the first band. The square lattice is found to be the most appropriate candidate to realize the ASC phenomenon. The bandwidth of the circular-void square lattice in the first band, however, is not sufficiently broad for practical applications. In Sec. 3, the bandwidth of ASC is enlarged by a factor of three by optimizing the shape of air voids. In Sec. 4, the ASC phenomenon is demonstrated by numerical simulations. At last, we summarize the paper in Sec. 5.

2. Dispersion discrepancy between TE and TM polarizations in 2D photonic crystals

In isotropic and uniform media, the dispersion properties for TE and TM polarizations are the same. In PhCs, however, they are always different due to the periodic modulation of dielectric medium. If only one polarization is required to be collimated in PhCs, the anisotropy of their EFCs, which is the fundamental ingredient to realize abnormal refraction, is the key issue to be considered. The anisotropy is significantly affected by the periodic modulation of the structure. There are normally two important factors to influence the modulation strength. The first one is the rotational symmetry of the photonic structure. Generally, lowering the symmetry leads to a more aberrance of the dispersion in the low photonic band and thus more obvious abnormal refraction. For example, the four-fold symmetry square lattice generally possesses a wider angular collimating range than a six-fold hexagonal structure in the first band. Reducing the symmetry further to a rectangular lattice can result in all-angle self-collimation [19]. The second factor is the filling factor, which should be in an appropriate range to achieve strong modulation in a specific structure. On the other hand, if one expects to realize self-collimation for both polarizations, another important issue, the similarity of the dispersion relation between TE and TM modes, needs to be taken into account. As self-collimation for one polarization has been realized in triangular, square and rectangular structures, we first compare the dispersion difference between TE and TM polarizations for these three typical 2D PhC structures.

Figure 1(a) depicts an example of the dispersion difference between TE and TM polarizations in the first band for the circular-void square lattice. The ratio between the radius of the circular-void and the lattice constant, r/a, is randomly chosen to be 0.3. A freely available software package was employed to obtain the fully-vectorial eigenmodes solution of Maxwell's [20]. Plane wave expansion (PWE) method with 4096 plane waves was used in all the calculations except specified. All the structures we consider in this paper consist of air voids immersed in a dielectric background with a dielectric constant of $\varepsilon=11.56$.

To compare the dispersion discrepancy (DD) between TE and TM polarizations over the irreducible Brillouin Zone (IBZ) for rectangular, square and triangular lattices of circular voids, we define DD in the following equations,

$$X_{ji} = (v_{TE})_{ji} - (v_{TM})_{ji}, \overline{X_j} = \frac{1}{n}\sum_{i=1}^{n} X_{ji}, j = 1...m \qquad (1)$$

$$S_j^2 = \frac{1}{n-1}\sum_{i=1}^{n} (X_{ji} - \overline{X_j})^2, j = 1...m \qquad (2)$$
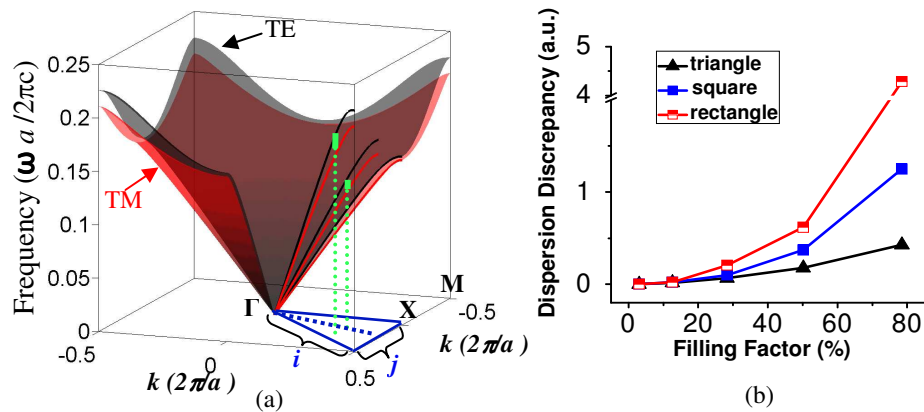
$$DD = (\sum_{j=1}^{m} S_j^2)/m, \qquad (3)$$

Fig. 1. (a) The sketch map of dispersion surfaces for TE and TM polarizations in the square lattice with r/*a*=0.3 in the first Brillouin Zone. The black surface stands for the TE mode and the red one for the TM mode. The vertical green bar represents the frequency difference at a specific k-vector. (b) The dispersion discrepancy in rectangular, square and triangular lattices versus the filling factor.

where ν_{TE}/ν_{TM} is the frequency of TE/TM mode and S^2 gives the sample variance. In the calculation, the IBZ is discretized into n×m computation points. n and m are set as 50 and 30 respectively to obtain a reasonably precise result. In order to keep the effective refractive index of the PhC constant, the filling factor for the three structures remains same when we scan r/*a*. The aspect ratio b/*a* of the rectangular lattice is 1.5, where b is the longer lattice vector and *a* is the shorter one. One thing need to be addressed is that the calculation of DD is based on the entire IBZ. This is reasonable since all the calculations start from the same point Γ and the dispersion relation for all the structures is linear at long wavelengths where EM waves cannot probe the fine structure of the crystal lattice [21]. The dispersion discrepancy in the self-collimating region can therefore be deduced directly by neglecting the linear part in the first band. Also need to be noted is that DD we define here is only applicable in the first band, where the dispersion relations for TE/TM are similar and relatively simple.

The quantitative results for DD versus the filling factor are shown in Fig. 1(b). As can be seen, the discrepancy in dispersions between TE and TM polarizations increases with the decrease of the rotational symmetry of three lattices. However, the difference is not apparent at smaller filling factors. When the filling factor falls below 12.6%, DD for the three lattices even becomes close to each other, implying that the dispersion properties are insensitive to structures. Obviously, the rectangular lattice has the largest dispersion discrepancy especially when the filling factor exceeds 50%. Hence, it is not an appropriate candidate to realize ASC although boasting the broadest angular collimating range for just one polarization. Therefore, it seems difficult to obtain a broad angular collimating range while remaining small discrepancy between TE and TM modes. A compromise may be the square lattice with proper filling factors because it possesses not only a relatively small DD but also a relatively broad angular range for self-collimation in the first band.

3. ASC Bandwidth in square-symmetry-based PhC structures with different voids

As pointed out in the above analysis, the square lattice with proper filling factors is the most appropriate candidate to realize ASC in the first photonic band. To judge the appearance of ASC in PhCs, we define three criteria: 1) the divergence of the energy propagation direction for TE and TM polarizations should be smaller than ±0.5° away from the ΓM direction; 2) the incident beams (from air) within ± 22.5° divergence should be able to be collimated for both polarizations; 3) no overlap exists between the first and second bands in order to avoid

multimodeness. Under these criteria, the frequency bandwidth ($\Delta\omega/\omega_o$, ω_o is the mid-frequency in the self-collimating region) of ASC for the normal circular-void square lattice is only 1.6%, which is not sufficient for practical applications. It is necessary to enlarge the bandwidth. Besides the rotational symmetry of the lattice, the shape of the void is another important factor to influence the dispersion relation of photonic structures. For example, by reducing the symmetry of the void, the absolute photonic band gap can be enlarged [22]. In this part, we will focus on investigating the influence of the void on the bandwidth of ASC in square-lattice-based structures.

First of all, the shape of the void influences the energy distribution in photonic structures. We calculate the distribution of the time-averaged electric-field (E-field) energy density, $\varepsilon|E|^2$, for square-lattice-based structures with different voids including circle, square, 45°-rotated-square, rectangle, ellipse and pill. As the self-collimating direction in the square lattice is along the ΓM direction in the first band, the difference between TE and TM polarizations at the M point (or M_2) is the largest among all the points along the ΓM direction. Therefore, we study the energy distribution at the M point. Furthermore, to obtain a ΓM-related symmetric angular range (for convenience), the long axis of the void is chosen to be collinear with the ΓM direction in all the calculations. The filling factor for different structures is kept the same as in the circular-void case with r/a=0.3. Figures 2 and 3 illustrate the calculation results for TM and TE modes, respectively. As can be seen, the energy distribution of the E-field does not change so much with different voids for the TM polarization. In the TE case, however, it is significantly influenced by the shape of the void.
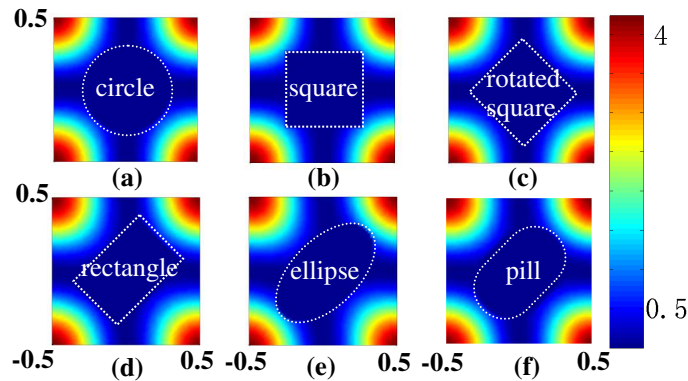

Fig. 2. The distributions of the time-averaged E-field energy density ($\varepsilon|E|^2$) for the TM mode at the M point in the first band of square-lattice-based structures with different voids. The unit of the length is in a. The white dotted lines depict the outlines of voids. The radius of the circular-void in (a) is arbitrarily chosen to be 0.3a. The filling factor for all the structures is kept the same as in (a). As can be seen, the energy density distributes similarly in all the structures.

In order to reduce the discrepancy in dispersions between TE and TM polarizations without decreasing the dispersion anisotropy, it is necessary to understand its underlying physics. Essentially, the dispersion difference between TE and TM modes in periodic structures can be correlated with the difference of their boundary condition at the void-dielectric interface. Normally, the magnetic-field (H-field) can be considered to be both normal- and tangent-continuous through interfaces in the nonmagnetic material for both polarizations as its relative permeability equals to 1. For the TM polarization in 2D PhCs, the E-field is parallel to the void-dielectric interface and tangent-continuous. It does not have any normal component. In the TE case, however, the boundary continuity situation is different. As the displacement field D is normal-continuous at the void-dielectric interface, the E-field is forced to cross both the low-ε and high-ε regions and thus non-continuous at the interface. Consequently, the discrepancy in dispersions appears between TE and TM modes. This is the

physical origin responsible for the narrow ASC bandwidth in the normal circular-void square-lattice structure.

As is known, the shape of the void can influence the bandwidth of the absolute PBG, it thus may be utilized to enlarge the ASC bandwidth by forcing the direction of the E-field to be coplanar in both polarizations. In Figs. 2 and 3, the shape of the void exhibits remarkable
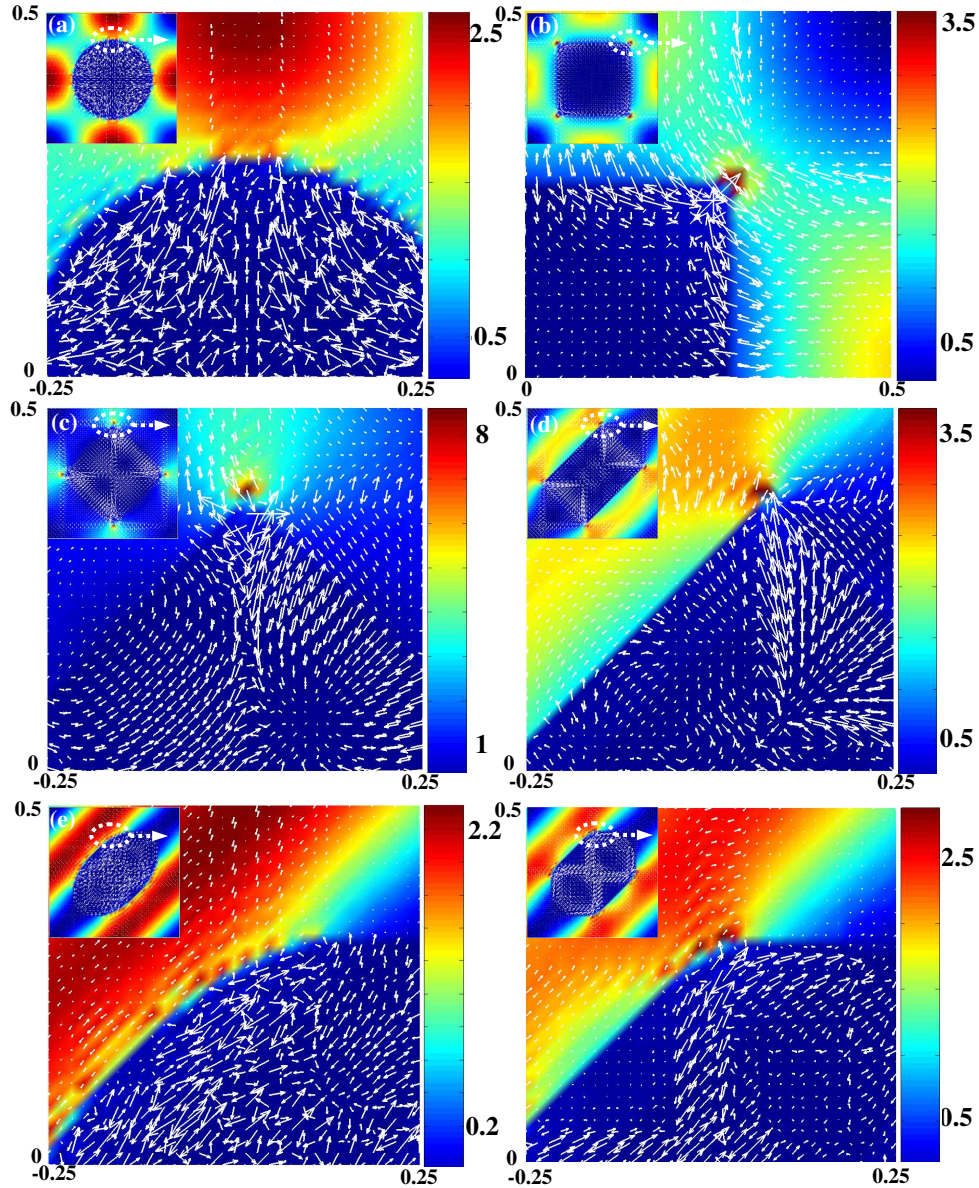

Fig. 3. The distributions of the time-averaged E-field energy density ($\varepsilon|E|^2$) for the TE mode. All the structural parameters are the same as in the Fig. 2. The white arrows stand for the in-plane E-field vectors. The insets in each figure stand for one lattice cell.

effect on the energy distribution of the E-field for the TE mode while ignorable effect on that for the TM mode, we thus try to adjust the direction of the E-field vector in the TE mode to imitate that in the TM mode. The white arrows in Fig. 3 depict the in-plane E-field vectors at the M point. Although the in-plane field is elliptically polarized in 2D photonic crystals, we

can apply the in-plane E-field vectors to approximately represent the elliptical polarization of each spatial point.

As the property of the E-field energy concentrated regions is the dominant factor to influence the dispersion relation in photonic structures [21], we mainly consider the E-field directions at those high energy areas. From Fig. 3(a), it can be seen that the E-field vectors are almost normal to the circular-void interfaces at the locations of the energy concentrated. Therefore, a large dispersion difference from the TM mode can be predicted. When the rotational symmetry of the void is reduced from isotropy to square, the E-field vector is forced to rotate away from the normal to the dielectric-void interface. Since we are discussing self-collimation along the ΓM direction, we rotate the square-void by 45° around its center and the energy is found to be concentrated at the corner either before or after the rotation. However, the direction of the E-field vector is different in both cases with respect to the void-dielectric interface. We then further reduce the rotational symmetry by changing the void to rectangle, ellipse and pill respectively, with the long axis along the ΓM direction. The energy is found to be distributed differently in each structure, as shown in Figs. 3(c)-3(f). The most remarkable feature is that the direction of the E-field vector is not the same in each structure at the high energy regions. For example, in the pill-void case (Fig. 3(f)), the E-field vectors are almost parallel to the void-dielectric interfaces within those areas enclosed by green dashed lines. As the E-field vector in the TM mode is also parallel to the void-dielectric interface, the pill-void structure is expected to posses the smallest discrepancy between TE and TM modes and thus boast the broadest ASC bandwidth among all the structures analyzed. One thing needs to be addressed is that simply reducing the symmetry of the void will not always work. For instance, the direction of the E-field vector is different when the square-void is rotated (refer to Figs. 3 (b) and 3(c). Therefore, the shape of the void has to be designed very carefully to obtain optimum result.
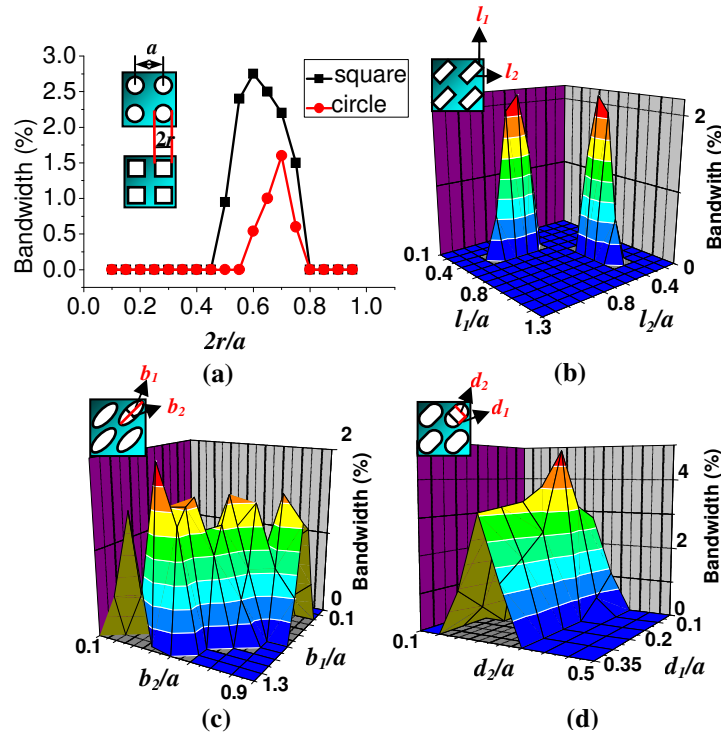

Fig. 4. The ASC bandwidth for square-lattice-based structures versus the filling factor. (a)-(d) is for circular-, rectangular-, elliptic- and pill-void structure, respectively. The specific shapes of each void are shown in the insets.

To verify the above analysis, we now calculate the bandwidth of ASC for square-lattice-based structures with different voids according to the three criteria we defined at the beginning of this part by the plane wave expansion (PWE) method. The results are shown in Fig. 4. The sketches of each structure are depicted in the insets. As can be seen, the broadest bandwidth for the circular-void structure is ~1.6% when its diameter 2r is 0.7a (Fig. 4(a)). In the square-void structure, the bandwidth reaches ~2.8% when its side length is 0.6a. This increase of the ASC bandwidth is consistent with the above analysis, in which the rotation of the E-field vector at the high energy locations in the square-void structure can reduce the discrepancy between TE and TM modes. When the square-void is rotated by 45° around the M point, the bandwidth of ASC shrinks to zero. If the length/width of the square-void, l_2/l_1, as shown in Fig. 4(b), is stretched to 2 (0.8 and 0.4 respectively) along the ΓM direction, the bandwidth can be extended to 2.1%. Tapering the void from rectangle to ellipse and pill along the ΓM direction can not only modify the bandwidth of ASC, but also increase the coupling efficiency at the input interface [23]. Figs. 4(c) and 4(d) exhibit the ASC bandwidth for elliptic- and pill-void structures with different filling factors. Apparently, it can be enlarged to ~4.8% in the pill-void structure when d_2=0.6a and d_1=0.2a. This bandwidth is three times of that in the circular-void structure. These results are consistent with our above analysis. Therefore, as we have pointed out in the above context, representing the elliptical polarization by the in-plane E-field vector is reasonable and does not distract our conclusion.

In order to present the underlying dispersion relationship of the ASC phenomenon in the pill-void structure, we now calculate its band structure and corresponding EFCs where ASC occurs. Fig. 5(a) illustrates its band structure for the four lowest photonic bands in the first BZ. The EFCs for both polarizations with d_2=0.6a and d_1=0.2a at frequencies of 0.182×2π c/a, 0.188×2π c/a and 0.191×2π c/a are given in Fig. 5(b). The black dashed lines represent the conservation lines of the k-vectors. The propagation direction in PhCs is marked by the yellow bulk arrow. As shown, incident beams within ±22.5^o divergence from normal to the input interface are able to be collimated along the ΓM direction in the frequency range from 0.182×2π c/a to 0.191×2π c/a for both polarizations. It is worth noting that the symmetry of EFCs is not four-fold anymore due to the non-symmetric elongation of the void. As the E-field energy of the TM mode is more concentrated in the dielectric region than that of the TE mode, the TM mode has a lower frequency than TE. Consequently, the angular collimating range for the TE mode is broader than that for the TM, as can be seen in Fig. 5(b).
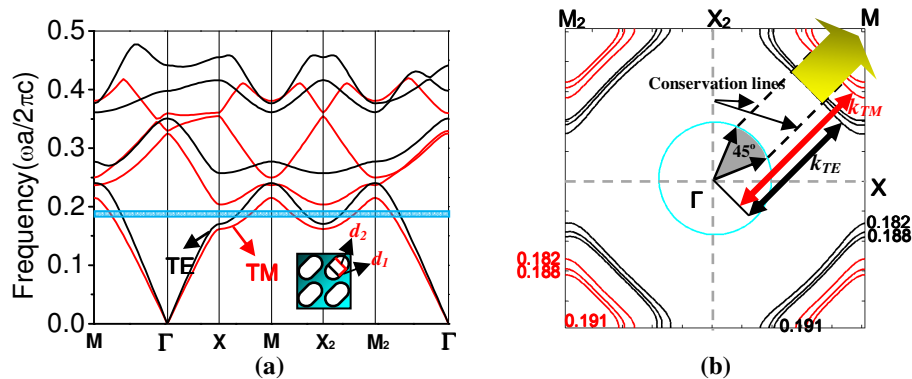

Fig. 5. The band structure (a) and EFCs (b) for the pill-void square lattice with d_2=0.6a, d_1=0.2a. The red/black color indicates TM/TE modes. The light blue box in (a) represents the operating region. The cyan circle is the light cone at a frequency of 0.188×2π c/a and the grey 45°- taper stand for the angular range for the incident k-vectors. As can be seen, the propagation direction of the energy, which is shown in the yellow bulk arrow, is along the ΓM direction in PhCs when the divergence of the incident beams is within 45° (i.e. ±22.5^o).

4. Spatial evolutions for the unpolarized self-collimation

In the above context, we have revealed how to enlarge the bandwidth of ASC in the first band by optimizing the shape of the void in the square-lattice-based structure. We now demonstrate the ASC effect by the finite-difference time-domain (FDTD) method as it is an intuitive and accurate tool to test the theoretical results in PhCs. The calculation area is $40\times100a$ with a grid size of $1/25a$. A Gaussian beam at a frequency of $0.188\times2\pi$ c/a (as an example) with a width of $4.1a$, which can emulate the $\pm22.5^{\circ}$ divergent input, was launched into PhCs perpendicularly.

Figs. 6(a) and 6(c) displays the E-/H-field distribution of the TM/TE mode to demonstrate the self-collimation phenomenon. As can be seen, the divergent incident beam is collimated along the ΓM direction without spreading even after propagating a distance as long as $100a$ for both polarizations. The absence of diffraction is also confirmed by the almost unchanged beam profiles before and after propagating in PhCs. The steady field distribution of E/H at the center of the beam is exhibited in Figs. 6(b) and 6(d). It is apparent that the transmittance remains approximately constant as a function of propagation distance, suggesting that the propagation loss is negligible for both polarizations. By optimizing the input interface as in the inset of Fig. 6(b), the transmission can reach 76% when normalized to the source for both polarizations. Considering the ASC phenomenon is realized in the first band here, a high transmission efficiency is expected in the application. Furthermore, if the device operates at 1550nm, the wavelength range for ASC can be broader than 70nm. Therefore, we expect that the ASC phenomenon realized in the pill-void square-lattice structure can find applications in future optical integrated circuits.
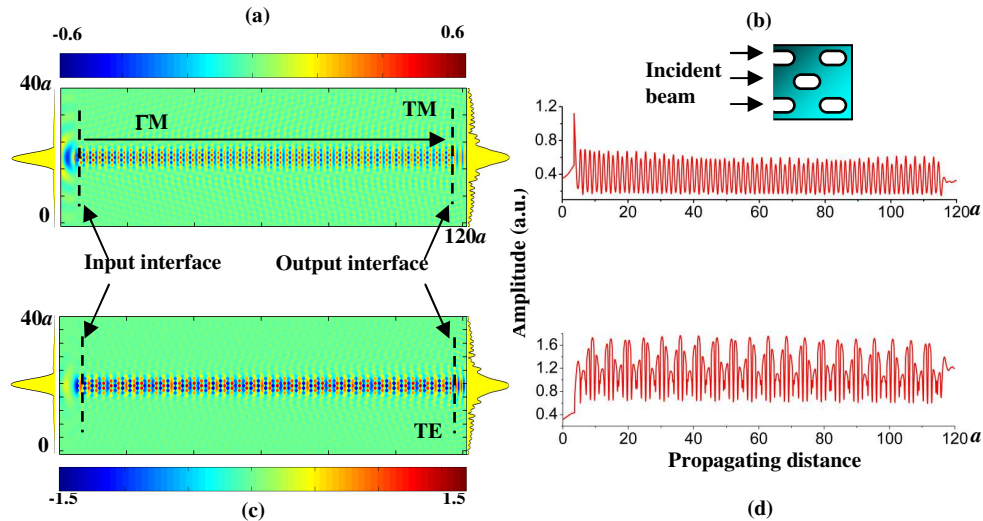

Fig. 6. The spatial evolutions of beams incident from air (left) into PhCs (right) for (a) TM and (c) TE polarizations at a frequency of $0.188\times2\pi$ c/a. The input interface shown in the inset has been modified to improve the transmission. The output medium is dielectric. (b) (d) The steady field distributions at different propagation distances. The oscillation of field distributions can be attributed to the modulation of the periodic PhC, in which the difference between TE and TM modes is due to the different length of the coupled k-vector along the ΓM direction (refer to k_{TE} and k_{TM} in the Fig. 5 (b)).

5. Summary

To conclude, we have investigated the dispersion properties of TE and TM polarizations for rectangular, square, triangular 2D photonic lattices and revealed how to find an appropriate PhC structure to realize the polarization-independent self-collimating effect in the first band.

The square lattice of pill-void was found to possess ~4.8% ASC bandwidth, which is the best candidate among all the structures analyzed. We attribute this enlargement to the rotation of the in-plane E-field vector in the TE polarization, which can reduce the dispersion discrepancy between both polarizations. Absolute self-collimation with negligible propagation loss and high transmission efficiency has been verified by numerical experiments. Such kind of function may find its role in future optical integrated circuits.

Acknowledgments